

Two-photon vibrational excitation of air by long-wave infrared laser pulsesJ. P. Palastro, J. Peñano, L. A. Johnson, and B. Hafizi
*Naval Research Laboratory, Washington, DC 20375-5346, USA*J. K. Wahlstrand and H. M. Milchberg
Institute for Research in Electronics and Applied Physics, University of Maryland, College Park, Maryland 20740, USA
(Received 17 June 2016; published 5 August 2016)

Ultrashort long-wave infrared (LWIR) laser pulses can resonantly excite vibrations in N_2 and O_2 through a two-photon transition. The absorptive vibrational component of the ultrafast optical nonlinearity grows in time, starting smaller than but quickly surpassing the electronic, rotational, and vibrational refractive components. The growth of the vibrational component results in a novel mechanism of third-harmonic generation, providing an additional two-photon excitation channel, fundamental + third harmonic. The original and emergent two-photon excitations drive the resonance exactly out of phase, causing spatial decay of the absorptive vibrational nonlinearity. This nearly eliminates two-photon vibrational absorption. Here we present simulations and analytical calculations demonstrating how these processes modify the ultrafast optical nonlinearity in air. The results reveal nonlinear optical phenomena unique to the LWIR regime of ultrashort pulse propagation in the atmosphere.

DOI: [10.1103/PhysRevA.94.023816](https://doi.org/10.1103/PhysRevA.94.023816)**I. INTRODUCTION**

Ultrashort laser pulses propagating through the atmosphere drive an ultrafast dielectric response by nonlinearly polarizing the constituent atoms and molecules [1–3]. For the primary constituents, the diatomic molecules N_2 and O_2 , the response consists of three motions: electronic, rotational, and vibrational. The time scale for each of these varies substantially and, when compared with the pulse duration or frequency, determines their dynamic contribution to the dielectric response.

Bound-electron dynamics occur on attosecond time scales $\tau_e \sim \hbar U_I^{-1}$ where U_I is the ionization potential. The electrons, as a result, respond nearly instantaneously to ultrashort (approximately femtosecond to picosecond) laser pulses with near-ultraviolet or longer periods (greater than femtoseconds). In contrast, the rotational and vibrational dynamics involve motion of the nuclei and occur on much longer time scales. The rotational motion has a characteristic time scale of picoseconds $\tau_r \sim \hbar^{-1} I_M$ where I_M is the moment of inertia [4–7]. Pulses with durations exceeding this adiabatically align the molecules and experience a near-instantaneous rotational response [4–7]. Much shorter pulses, on the other hand, impulsively align the molecules and experience a delayed rotational response [4–7]. A similar transition from an instantaneous to a delayed response occurs during vibrational excitations but at much shorter pulse durations [8–12]. The vibrational motion occurs on the few femtosecond time scale $\tau_v \sim \Omega_v^{-1}$ where Ω_v is the vibrational frequency, and thus, near-infrared pulses must be close to the single cycle for impulsive excitation [8–12].

Although a nonadiabatic vibrational excitation can be achieved with few-cycle pulses, there is another option: using a longer wavelength pulse. Neither N_2 nor O_2 possess a permanent dipole moment; the laser-pulse-driven rotation and vibration are mediated, instead, by an induced dipole. At the quantum level, the induced dipole interaction corresponds to a two-photon process by which the laser pulse excites coherence between two (selection rule allowed) rotational or vibrational states. For pulses with frequencies incommensurate with the

states' transition frequency, the pulse duration determines the dynamics as described above. However, when the frequency equals half the transition frequency, the pulse resonantly excites coherence between the states. Specifically, long-wave infrared (LWIR) pulses with wavelengths near $\lambda = 4\pi c/\Omega_v$, 8.4 or 12.6 μm for N_2 or O_2 , respectively [13] will resonantly excite vibrational coherence. Even with the recent popularity of midinfrared (MIR) ultrashort pulse propagation studies [14–18], the effect of this excitation on propagation, either on- or off-resonance, has yet to be examined.

Here we consider the ultrafast two-photon vibrational excitation of N_2 and O_2 and examine its effect on LWIR pulse propagation. We find that the absorptive vibrational component of the ultrafast optical nonlinearity grows in time, starting smaller than but quickly surpassing the electronic, rotational, and vibrational refractive components. The growth of the vibrational component results in a novel mechanism of accelerated third-harmonic generation. The resulting third harmonic provides an additional resonant two-photon excitation channel, fundamental + third harmonic. The original and emergent two-photon excitations drive the vibrational resonance exactly out of phase with each other, causing spatial decay of the absorptive vibrational nonlinearity. That is: co-propagation of the fundamental and the resonantly generated third harmonic nearly eliminates two-photon vibrational absorption. Both simulations and analytical calculations are presented demonstrating how these processes modify the ultrafast optical nonlinearity in air.

II. ULTRAFAST OPTICAL NONLINEARITY OF AIR

The nonlinear polarization density induced by laser pulses propagating through the atmosphere $P = P_e + P_r + P_v$ includes contributions from the electronic P_e , rotational P_r , and vibrational P_v responses of (predominately) N_2 and O_2 molecules. Unless otherwise stated, a sum over the N_2 and O_2 polarizations, weighted by number density, is implied. Bound electrons respond near instantaneously to LWIR pulses such that the electronic polarization can be expressed as

TABLE I. Parameters for nonlinear polarization.

Parameter	Reference	N ₂	O ₂
Fraction		0.8	0.2
$n_2(\text{m}^2/\text{W})$	[6,16]	7.3×10^{-24}	9.3×10^{-24}
$\Omega_v(\text{s}^{-1})$	[12]	4.5×10^{14}	3.0×10^{14}
$I_M(\text{J s}^2)$	[4]	1.46×10^{-46}	1.9×10^{-46}
$\Delta a(\text{m}^3)$	[6]	6.7×10^{-31}	10.2×10^{-31}
$\mu(\text{kg})$		1.2×10^{-26}	1.3×10^{-26}
$\partial a/\partial Q(\text{m}^2)$	[20]	1.75×10^{-20}	1.46×10^{-20}

$P_e = \varepsilon_0 \chi_e E$ where

$$\chi_e = 4c\varepsilon_0 n_2 E^2/3 \quad (1)$$

is the electronic susceptibility, E is the transverse electric field of a linearly polarized laser pulse, and n_2 is the second-order nonlinear refractive index [19]. The values of n_2 and other parameters required for calculating the polarizations are summarized in Table I.

The rotational and vibrational polarizations are derived using density-matrix theory. Here we summarize the derivation and refer the reader to Refs. [5,12,21,22] for additional details. The molecules are modeled as spring-bound atom pairs with an anisotropic polarizability that varies with atomic separation. This allows a laser pulse to both align and stretch the molecules. The calculation involves expanding the density matrix in orders of the field-dependent potential responsible for the alignment and stretching. To lowest order in the expansion, alignment or stretching corresponds to excitation of coherence between two rotational or vibrational states, respectively. At this order, no change in the state populations occurs.

In the absence of a field, the rovibrational energy is given by $U_{nj} = \hbar\Omega_v(n + \frac{1}{2}) + \frac{1}{2}\hbar^2 I_M^{-1} j(j+1)$, where n and j , respectively, are the vibrational and total angular momentum quantum numbers, Ω_v is the vibration frequency, and I_M is the moment of inertia. Assuming thermodynamic equilibrium, the zeroth-order density matrix is then given by $\rho_{n_{jm},j,m}^0 = \delta_{n_{jm},n_{jm}} Z_p^{-1} D_j \exp[-U_{nj}/T]$, where m is the angular momentum quantum number along the pulse polarization axis, T is the temperature, D_j is a degeneracy factor associated with nuclear spin, and $Z_p = \sum_{n_j} (2j+1) D_j \exp[-U_{nj}/T]$ is the partition function. A linearly polarized laser pulse drives coherence between rotational or vibrational states separated by $\Delta j = \pm 2$ or $\Delta n = \pm 1$, respectively. The resulting rotational polarization can be expressed as $P_r = \varepsilon_0 \sum_j \chi_{r,j} E$, where

$$\left(\frac{\partial^2}{\partial t^2} + \omega_{j,j-2}^2 \right) \chi_{r,j} = -\frac{32\pi^2 \varepsilon_0 \eta (\Delta\alpha)^2}{15 I_M} j(j-1) \times \left(\frac{\rho_{j,j}^0}{2j+1} - \frac{\rho_{j-2,j-2}^0}{2j-3} \right) E^2, \quad (2)$$

$\omega_{j,j-2} = \hbar I_M^{-1} (2j-1)$, η is the number density, $\Delta\alpha$ is the polarizability anisotropy, and $\rho_{j,j}^0 = \sum_{nm} \rho_{n_{jm},n_{jm}}^0$. Similarly, the vibrational polarization can be expressed as $P_v = \varepsilon_0 \chi_v E$, where

$$\left(\frac{\partial^2}{\partial t^2} + \Omega_v^2 \right) \chi_v = \frac{4\pi^2 \varepsilon_0 \eta}{\mu} \left(\frac{\partial \alpha}{\partial Q} \right)^2 E^2, \quad (3)$$

μ is the reduced atomic mass, and $\partial\alpha/\partial Q$ is the change in isotropic polarizability with atomic separation.

The full rovibrational response has been simplified in Eqs. (2) and (3) by applying the following observations. First, the molecules largely populate the ground vibrational state at atmospheric temperatures. Second, contributions proportional to $\partial\Delta\alpha/\partial Q$, including simultaneous rotational-vibrational excitations, contain factors making them an order of magnitude smaller than terms proportional to $\partial\alpha/\partial Q$. Finally, the time between geometric cross-section-based collisions far exceeds the excitation times of interest.

III. TWO-PHOTON VIBRATIONAL RESONANCE

Equations (2) and (3) admit resonant solutions: When the period of E^2 is commensurate with the oscillator period, the molecular susceptibility undergoes temporal growth. The rotational resonances reside in the terahertz range, accessible by beating two laser frequencies together or by appropriately delaying optical pulses [22]. Of interest here is the two-photon vibrational resonance accessible by LWIR pulses with wavelength $\lambda_L = 4\pi c/\Omega_v$: 8.4 or 12.6 μm for N₂ or O₂, respectively.

To determine the solution to Eq. (3), we express the laser pulse electric field as a plane wave modulating an envelope $E = \hat{E}(t) \sin(\omega_L t + \phi)$. Resonant excitation requires a nonimpulsive drive in which the pulse duration, σ , far exceeds the vibrational period, $\sigma\Omega_v \gg 1$. The solution to Eq. (3) can then be expressed as $\chi_v = \chi_{v0} + \chi_{v+} + \chi_{v-}$, where

$$\chi_{v0} \simeq \frac{\gamma \hat{E}^2(t)}{2\Omega_v^2}, \quad (4)$$

$$\chi_{v+} \simeq -\frac{\gamma \hat{E}^2(t)}{4\Omega_v(\Omega_v + 2\omega_L)} \cos(2\omega_L t + 2\phi), \quad (5)$$

$$\chi_{v-} = -\frac{\gamma}{4\Omega_v} \int_{-\infty}^t \sin[\Omega_v t - (\Omega_v - 2\omega_L)t' + 2\phi] \hat{E}^2(t') dt', \quad (6)$$

and $\gamma = 4\pi^2 \varepsilon_0 \eta \mu^{-1} (\partial_Q \alpha)^2$. Equations (4)–(6) contribute to polarizations that oscillate either in phase or in quadrature with the laser field. The in phase, or refractive, components modify the phase of the pulse during propagation, whereas the quadrature, or absorptive, components modify the amplitude. Equation (4), for instance, results in the refractive polarization,

$$P_{v0} = \frac{\gamma \hat{E}^2(t)}{2\Omega_v^2} \hat{E}(t) \sin(\omega_L t + \phi). \quad (7)$$

Equation (5) also results in a refractive polarization at ω_L ,

$$P_{v+} = \frac{\gamma \hat{E}^2(t)}{8\Omega_v(\Omega_v + 2\omega_L)} \hat{E}(t) [\sin(\omega_L t + \phi) - \sin(3\omega_L t + 3\phi)], \quad (8)$$

but includes an additional component oscillating at $3\omega_L$ that contributes to the usual source of third-harmonic generation in air.

Equation (6) captures the resonant response of the vibrational excitation. The resulting polarization exhibits two behaviors depending on the size of the detuning $\Delta = \omega_L -$

$\frac{1}{2}\Omega_v$ relative to the pulse bandwidth σ^{-1} . For large detuning $\sigma|\Delta| \gg 1$, the polarization is primarily refractive. The refractive component at ω_L is

$$P_{v-} \simeq \frac{\gamma \hat{E}^2(t)}{8\Omega_v(\Omega_v - 2\omega_L)} \hat{E}(t)[\sin(\omega_L t + \phi) - \sin(3\omega_L t + 3\phi)]. \quad (9)$$

As with Eq. (8), the $3\omega_L$ component contributes to usual third-harmonic generation. The coefficient $\gamma \hat{E}^2(t)/16 \Delta \Omega_v$, changes signs across the resonance, which we discuss further below. For small detuning $\sigma|\Delta| \ll 1$, the laser frequency is near resonant, and χ_{v-} undergoes the temporal growth characteristic of a resonantly driven harmonic oscillator. In this limit, the resulting polarization is primarily absorptive,

$$P_{v-} = -\frac{\gamma}{8\Omega_v} \left(\int_{-\infty}^t \hat{E}^2(t') dt' \right) \hat{E}(t)[\cos(\omega_L t + \phi) - \cos(3\omega_L t + 3\phi)], \quad (10)$$

and scales with the accumulated laser fluence in contrast to Eqs. (7)–(9) which scale with $\hat{E}^2(t)$. The $3\omega_L$ component of Eq. (10) provides a novel source for third-harmonic generation far more efficient than that provided by Eqs. (8) and (9). As we will see, this term plays an important role in the self-consistent evolution of the laser pulse and vibrational response.

The effective complex susceptibilities at ω_L can be extracted from Eqs. (7)–(10). In particular, we write $\langle \chi_j \rangle = \langle \chi_j^R \rangle + i \langle \chi_j^A \rangle$, where $j = e, r$, or v , $\langle \chi_j^R \rangle \equiv \langle [\sin(\omega_L t + \phi) P_j] / [\sin(\omega_L t + \phi) E] \rangle$, $\langle \chi_j^A \rangle \equiv -\langle [\cos(\omega_L t + \phi) P_j] / [\sin(\omega_L t + \phi) E] \rangle$, $\langle \rangle$ denotes a cycle average, and the superscripts R and A refer to refractive and absorptive, respectively. In the refractive limit $\sigma|\Delta| \gg 1$,

$$\langle \chi_v \rangle = \frac{\gamma \hat{E}^2(t)}{2\Omega_v^2} + \frac{\gamma \hat{E}^2(t)}{8\Omega_v(\Omega_v + 2\omega_L)} + \frac{\gamma \hat{E}^2(t)}{8\Omega_v(\Omega_v - 2\omega_L)}. \quad (11)$$

Equation (11) is the standard vibrational response in the near-infrared frequency range of $\omega_L \gg \Omega_v$. The first term $\gamma \hat{E}^2(t)/2\Omega_v^2$ tracks the pulse intensity and contributes to the instantaneous Kerr nonlinearity in air. To avoid double counting this contribution in the total polarization, the n_2 values measured in Refs. [7,17], which include both the electronic and the vibrational contributions, have been adjusted in Table I to only include the electronic contribution $n_2 \rightarrow n_2 - (3\pi^2 \eta / c \Omega_v^2 \mu) (\partial \alpha / \partial Q)^2$. The second and third terms in Eq. (11) contribute minimally for near-infrared frequencies.

At LWIR frequencies, the third term, the resonant vibrational response, becomes the dominant refractive contribution. Just above resonance, this term is negative $\sim -\gamma \hat{E}^2(t)/16\Omega_v \Delta$. One might suppose that with a small enough detuning the second term could negate the nonlinear rotational and electronic responses. In practice, however, the minimum is limited to $\sim -\gamma \hat{E}^2(t)\sigma/16\Omega_v$ before the response becomes largely absorptive. In the absorptive limit $\sigma|\Delta| \ll 1$,

$$\langle \chi_v \rangle = \frac{\gamma \hat{E}^2(t)}{2\Omega_v^2} + \frac{\gamma \hat{E}^2(t)}{8\Omega_v(\Omega_v + 2\omega_L)} + i \frac{\gamma}{8\Omega_v} \left(\int_{-\infty}^t \hat{E}^2(t') dt' \right), \quad (12)$$

with the last term providing the largest by magnitude contribution; recall $\sigma \Omega_v \gg 1$.

IV. NEAR-RESONANT LWIR PROPAGATION

To simulate the resonant two-photon vibrational excitation and its effect on propagation, we use the one-dimensional (1D) scalar unidirectional pulse propagation equation (UPPE) [23,24]. The UPPE equation evolves each frequency component of the pulse independently. This avoids slowly varying envelope approximations, making it ideal for situations in which harmonic generation and high-order dispersion are important. Backwards propagation is, however, neglected. In a frame co-propagating with the laser pulse along the Cartesian z axis, the transverse electric field evolves according to

$$\frac{\partial}{\partial z} \hat{E}(z, \omega) = ik(\omega) \left[1 - \frac{c}{n(\omega)v_f} \right] \hat{E}(z, \omega) + \frac{i\omega}{2c\epsilon_0 n(\omega)} \hat{P}(z, \omega), \quad (13)$$

where “ $\hat{}$ ” indicates a frequency domain quantity, ω is the conjugate variable to the moving frame coordinate $\tau = t - z/v_f$, v_f is the frame velocity, $k(\omega) = n(\omega)\omega/c$, $n(\omega)$ is the linear refractive index, and P is the nonlinear polarization calculated with Eqs. (1)–(3). We choose the frame velocity equal to the group velocity at the carrier frequency ω_L : $v_f = c/[n + \omega \partial_\omega n]|_{\omega_L}$, where $n(\omega)$ is calculated using an empirical formula for air provided in Ref. [25]. The Appendix details the validity conditions for the 1D propagation model.

In the simulations, the temporal pulse profile was initialized as $E(0, \tau) = E_L \sin(\omega_L \tau) e^{-\tau^2/\sigma^2}$, where $\sigma = 850$ fs corresponds to a 1-ps intensity FWHM duration. The amplitude E_L was chosen to give a peak intensity $I = \frac{1}{2} c \epsilon_0 E_L^2$ of 1×10^{12} W/cm². For LWIR wavelengths, this intensity results in minimal ionization, justifying the absence of a free-electron current in Eq. (13). Specifically, the fractional ionization is expected to be less than 10^{-10} based on the ionization rate presented in Ref. [26] with parameters from Ref. [27].

Figure 1 displays the effective susceptibilities as a function of time after 15 cm of propagation. Examples of below-resonance $\lambda_L = 8.52\text{-}\mu\text{m}$, resonant $\lambda_L = 8.37\text{-}\mu\text{m}$, and above-resonance $\lambda_L = 8.22\text{-}\mu\text{m}$ N₂ vibrational excitations are shown from left to right, respectively. For reference, the pulse intensity profile follows the effective electronic susceptibility $\langle \chi_e \rangle$. At each wavelength, the refractive vibrational susceptibility is smaller in magnitude than the electronic and rotational susceptibilities, and as expected from Eq. (11), it switches signs across the resonance. On-resonance, the absorptive vibrational susceptibility undergoes the rapid temporal growth characteristic of a resonantly driven harmonic oscillator, surpassing the electronic and rotational susceptibilities in amplitude. At the quantum level, the laser pulse has resonantly driven coherence between the ground and the first excited vibrational states. Nevertheless, the net population in the first excited vibrational state remains low, consistent with our approximation to exclude additional vibrational states in Eq. (3). In particular, one can use the density-matrix expansion [12] to find the condition for small

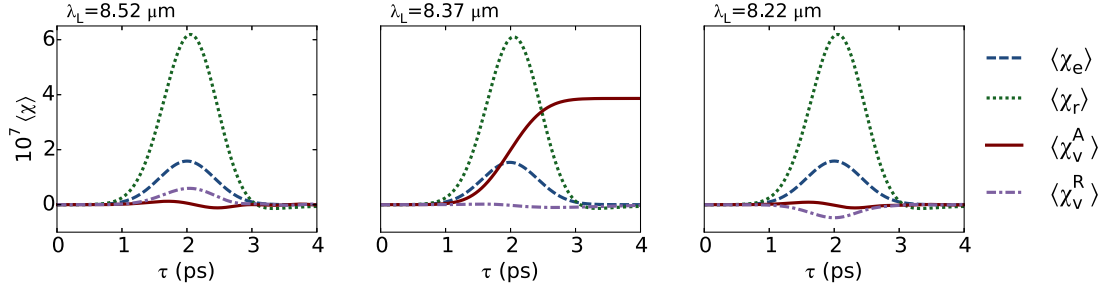


FIG. 1. Amplitude of the effective electronic (blue dashed curve), rotational (green dotted curve), absorptive (red solid curve), and refractive (purple dashed-dotted curve) vibrational susceptibilities as a function of pulse frame coordinate after 15cm of propagation. From left to right the plots show examples of below-resonant, resonant, and above-resonant excitations, respectively.

population transfer: $(\mu\hbar\Omega_v)^{-1}[\pi\epsilon_0(\partial_Q\alpha)\tau E_L^2]^2 \ll 1$, which for the parameters considered here evaluates to 0.02.

Figure 2(a) shows the resonantly driven absorptive vibrational susceptibility over a 3-m propagation path. As in Fig. 1, the response grows in time but quickly decays as the pulse propagates through space. This can be seen clearly in Fig. 2(b), which displays $\langle\chi_v^A\rangle$ at $\tau = 4$ ps on the bottom horizontal axis as a function of propagation distance [shared vertical axis with Fig. 2(a)]. Examination of Eq. (3) might lead one to believe that the spatial decay of $\langle\chi_v^A\rangle$ results from a decrease in the pulse fluence due to depletion. Surprisingly, however, the fluence remains nearly constant during the spatial decay as demonstrated by the dashed line, top horizontal axis, in Fig. 2(b).

V. ANALYSIS OF VIBRATIONAL RESPONSE EVOLUTION

The source of the spatial decay and the self-consistent evolution of the resonant vibrational excitation can be illustrated

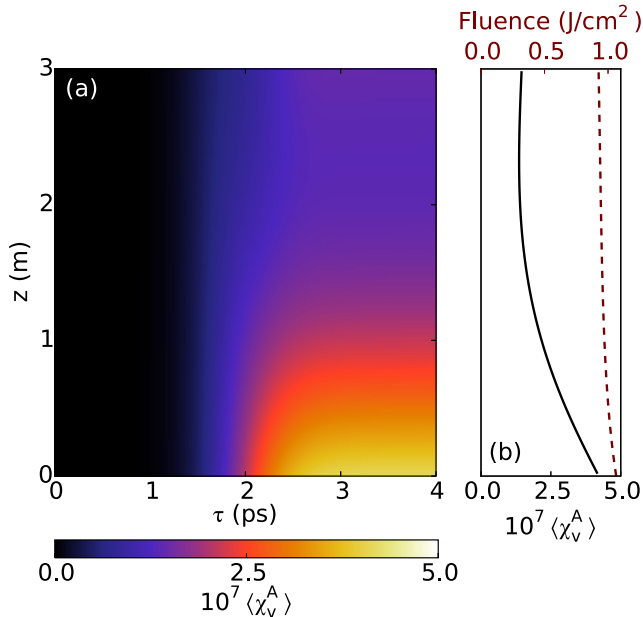


FIG. 2. (a) Resonant absorptive vibrational susceptibility as a function of pulse frame coordinate and propagation distance. (b) Resonant absorptive vibrational susceptibility at $\tau = 4$ ps (black solid curve and bottom horizontal axis) and total pulse fluence (red dashed curve and top horizontal axis) as a function of propagation distance.

using a reduced multiscale analytical model. We limit the analysis to the evolution of the laser pulse, governed by the wave equation and the vibrational response:

$$\left(\frac{\partial^2}{\partial z^2} - \frac{2}{c} \frac{\partial^2}{\partial \tau \partial z}\right)E = \frac{1}{c^2} \frac{\partial^2}{\partial \tau^2} \chi_v E, \quad (14)$$

$$\left(\frac{\partial^2}{\partial \tau^2} + \Omega_v^2\right)\chi_v = \gamma E^2. \quad (15)$$

The multiscale analysis involves expanding Eqs. (14) and (15) in time and spatial scales by writing $\partial_\tau = \partial_{\tau_0} + \epsilon \partial_{\tau_1} + \dots$, $\partial_z = \partial_{z_0} + \epsilon \partial_{z_1} + \dots$, $\chi_v(z, \tau) = \sum_n \epsilon^n \chi_{vn}(z_0, z_1, \dots; \tau_0, \tau_1, \dots)$, $E(z, \tau) = \sum_n \epsilon^n E_n(z_0, z_1, \dots; \tau_0, \tau_1, \dots)$, and $\gamma = \epsilon^2 \hat{\gamma}$. As we will demonstrate, the spatial decay results from resonant third-harmonic generation, motivating our expression for the electric field,

$$E_0 = A \sin(\omega_L \tau_0 + \phi) + B \sin(3\omega_L \tau_0 + 3\phi), \quad (16)$$

where $\omega_L = \frac{1}{2}\Omega_v$ and the dependence of A , B , and ϕ on z_1 and τ_1 is implied. Consistent with Eq. (16), we set the lowest-order vibrational response to zero $\chi_{v0} = 0$.

Upon performing the expansion and keeping only resonant terms in χ_v , we find the following:

$$\chi_v = -2\langle\chi_v^A\rangle \sin(\Omega_v \tau + 2\phi), \quad (17)$$

$$\frac{\partial A}{\partial z} = -\frac{\Omega_v}{4c} \langle\chi_v^A\rangle (A + B), \quad (18)$$

$$\frac{\partial B}{\partial z} = \frac{3\Omega_v}{4c} \langle\chi_v^A\rangle A, \quad (19)$$

where $\langle\chi_v^A\rangle = \gamma F(\tau)/4\Omega_v c \epsilon_0$, $F(\tau) = \frac{1}{2} c \epsilon_0 \int_{-\infty}^{\tau} A(A - 2B) d\tau'$, and we have dropped the subscripts on z and τ . The source of third-harmonic generation, the right-hand side of Eq. (19), results from the beating of χ_v with the fundamental oscillations of the laser pulse $\omega + \Omega_v = 3\omega$. The second right-hand side term of Eq. (18) $\propto \langle\chi_v^A\rangle B$ accounts for depletion of the fundamental during this process, whereas the first term $\propto \langle\chi_v^A\rangle A$ accounts for depletion from vibrational excitation. A simple scaling for the spatial decay length of $\langle\chi_v^A\rangle$ can be found by deriving perturbation solutions for Eqs. (18) and (19): $A \simeq A_0 + \delta A$, $B \simeq B_0 + \delta B$, and $F = F_0 + \delta F$. The pulse starts with no initial third-harmonic content such that $B_0 = 0$. Setting $A_0 = E_L e^{-\tau^2/\sigma^2}$, we have $\delta A = -(\gamma z/16c^2\epsilon_0)A_0 F_0$, $\delta B = (3\gamma z/16c^2\epsilon_0)A_0 F_0$, $F_0(\tau) = (F_L/2)[1 + \text{erf}(2^{1/2}\tau/\sigma)]$, and $F_1(\tau) = -(\gamma z/4c^2\epsilon_0)F_0^2$, where $F_L = \frac{1}{2} c \epsilon_0 (\pi/2)^{1/2} \sigma E_L^2$ is

the initial pulse fluence. Well after the pulse, the amplitude of the vibrational susceptibility is then

$$\langle \chi_v^A \rangle = \left(\frac{\gamma F_L}{4\Omega_v c \varepsilon_0} \right) \left(1 - \frac{z}{Z_d} \right), \quad (20)$$

which spatially decays over the length scale $Z_d = 4c^2 \varepsilon_0 / \gamma F_L$.

Equations (17)–(19) and the solutions above capture several features observed in the simulations. Foremost, the laser pulse resonantly excites coherence between the ground and first excited vibrational states through a two-photon transition. This results in an absorptive vibrational susceptibility Eq. (17) that oscillates at twice the fundamental laser frequency with an amplitude $\langle \chi_v^A \rangle$ that grows in time. The growth of $\langle \chi_v^A \rangle$, in turn, accelerates the third-harmonic generation, evident in the presence of $\langle \chi_v^A \rangle$ on the right-hand side of Eq. (19). The presence of the third harmonic opens an additional two-photon channel for resonant vibrational excitation $3\omega_L - \omega_L = \Omega_v$. This emergent excitation channel drives the vibrational resonance exactly out of phase with the $\omega_L + \omega_L = \Omega_v$ excitation. Symbolically, the $\omega_L + \omega_L = \Omega_v$ and $3\omega_L - \omega_L = \Omega_v$ excitation channels correspond to the first $\propto A^2$ and second $\propto -AB$ terms in $\langle \chi_v^A \rangle \propto F \propto \int^\tau A(A - 2B)d\tau'$, respectively. As the fundamental amplitude depletes $\delta A \propto -z$ and the third-harmonic amplitude grows $\delta B \propto z$, the vibrational susceptibility spatially decays, Eq. (20).

In support of this explanation, Fig. 3 displays the normalized fluence of the third harmonic resulting from off- and on-resonant pulses $\lambda_L = 8.57$ and $8.37 \mu\text{m}$, respectively. The fluences are normalized by the total pulse fluence such that the value represents the fraction contributed by the third harmonic. Consistent with the analysis above, the resonant vibrational excitation accelerates third-harmonic generation, reaching a value >3 times that of the off-resonant pulse after 3m, with a conversion efficiency of $\sim 30\%$. We note that for the parameters considered here, higher-order harmonics, while present, did not reach amplitudes sufficient to significantly affect propagation or the vibrational excitation.

Even in light of Fig. 3, the interpretation offered by the multiscale analysis remains qualitative. For further validation, we simulated the propagation with Eq. (13) but included

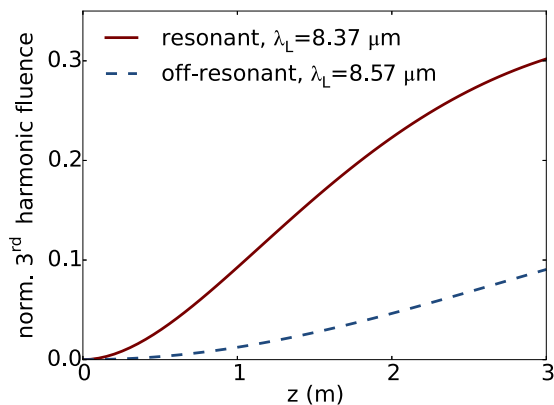


FIG. 3. Normalized fluence of the third harmonic as a function of propagation distance for resonant (red solid curve) and off-resonant (blue dashed curve) vibrational excitations. The values are normalized to the total fluence of the pulse.

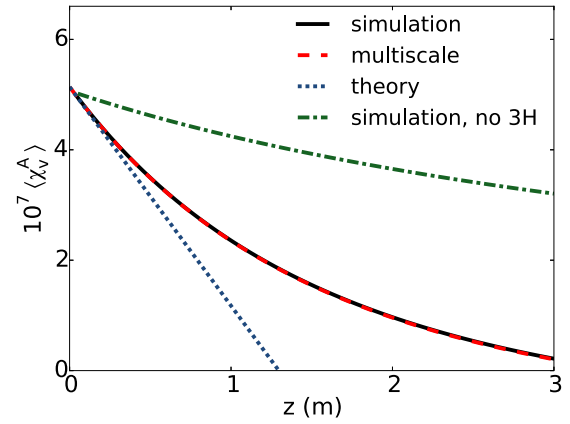


FIG. 4. Resonant absorptive vibrational susceptibility as a function of propagation distance at $\tau = 4$ ps. The solid black, red dashed, and blue dotted curves show the results from the simulation including only the N_2 vibrational nonlinearity, the multiscale calculation, and the perturbation solution Eq. (10), respectively. The green dashed-dotted line displays the result of the simulations when third-harmonic generation is suppressed.

only the N_2 vibrational polarization density: dispersion, O_2 nonlinearities, and N_2 electronic and rotational nonlinearities were omitted. The N_2 density fraction was increased to 1.0 accordingly. Figure 4 compares the resulting $\langle \chi_v^A \rangle$ at $\tau = 4$ ps with that calculated from the numerical solutions to Eqs. (18) and (19) and the perturbation result Eq. (20). The pulse parameters were identical to those above. The figure clearly exhibits agreement between the simulation and the analysis, where as expected, the perturbation result agrees only for short distances.

Figure 4 also shows $\langle \chi_v^A \rangle$ when third-harmonic generation is suppressed in the simulations (achieved by only evolving frequencies satisfying $\omega \leq 2\omega_0$). The spatial decay is less severe in this case and results solely from a decrease in the pulse fluence due to two-photon vibrational absorption. Figure 5 displays this decrease. Depletion of the pulse fluence

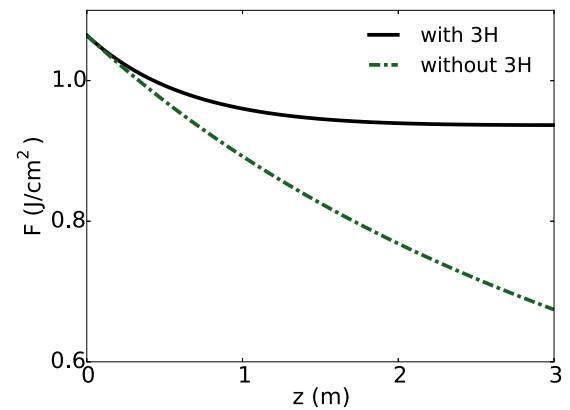


FIG. 5. Pulse fluence as a function of propagation distance. The solid black and green dashed-dotted lines show the results with and without third-harmonic generation in the simulations including only the N_2 vibrational nonlinearity. The resonant third-harmonic generation contributes to the near elimination of two-photon vibrational absorption.

in the presence of third-harmonic generation is also displayed. The solid and dashed-dotted curves correspond to the same curves in Fig. 4. With resonant third-harmonic generation, the two-photon vibrational absorption is nearly eliminated, and the fluence plateaus. Without third-harmonic generation, the fluence continues to drop due to vibrational absorption. Figures 4 and 5 clearly demonstrate that the spatial decay of $\langle \chi_v^A \rangle$ results from the out-of-phase contribution of the $3\omega_L - \omega_L = \Omega_v$ excitation, enabled by the accelerated third-harmonic generation.

It is worth noting that this cancellation phenomenon occurs, in part, because of the weak atmospheric dispersion at LWIR and MIR wavelengths. As a comparison, the distance for phase walk off between the fundamental and the third-harmonic $L = [n(\omega_L) - n(3\omega_L)]^{-1}(\lambda_L/6)$ of a $\lambda_L = 8.4\text{-}\mu\text{m}$ pulse is $\sim 8\text{m}$, whereas that of a $\lambda_L = 800\text{-nm}$ pulse is only $\sim 6\text{mm}$ [25]. The weak LWIR dispersion allows for the extended nonlinear interaction of the fundamental and third harmonic.

VI. SUMMARY AND CONCLUSIONS

We have examined the two-photon vibrational excitation of air molecules by ultrashort LWIR laser pulses. A specific example of resonant excitation of N_2 with a $\lambda_L = 8.37\text{-}\mu\text{m}$ pulse was presented. Simulations and analytical calculations demonstrated that the absorptive vibrational susceptibility undergoes temporal growth, characteristic of a resonantly driven harmonic oscillator. Although the vibrational response typically contributes only a small fraction of the optical nonlinearity, the absorptive contribution surpassed both the electronic and the rotational nonlinearities when driven by a 1-ps $1 \times 10^{12}\text{-W/cm}^2$ pulse. The temporal growth of the susceptibility was shown to accelerate third-harmonic generation, providing an additional two-photon excitation channel $3\omega_L - \omega_L = \Omega_v$. This additional channel drives the vibrational susceptibility exactly out of phase with the original $\omega_L + \omega_L = \Omega_v$ channel, resulting in spatial decay of the absorptive vibrational response. The same effects, although not

presented, occur during the excitation of O_2 by $\lambda_L = 12.6\text{-}\mu\text{m}$ pulses.

ACKNOWLEDGMENTS

The authors would like to thank M. Helle, Y.-H. Chen, and A. Stamm for fruitful discussions. This work was supported by the Naval Research Laboratory 6.1 Base Program. J.K.W. and H.M.M. acknowledge the support of the Air Force Office of Scientific Research (Grant No. FA95501310044), the National Science Foundation (Grant No. PHY1301948), and the Army Research Office (Grant No. W911NF1410372).

APPENDIX: CONDITIONS ON 1D PROPAGATION

Validity of the 1D simulation and its correspondence with potential experiments requires an initial spot size large enough that the pulse remains collimated during propagation. As a rough validity condition, we write $(Lw_0^{-1})|\partial_z w| \ll 1$, where w is the e^{-2} radius of a Gaussian intensity profile with initial value w_0 and L is the propagation distance. Weak dispersion at LWIR wavelengths and the relatively small bandwidth of the pulses considered here $\omega_0\sigma \gg 1$ minimize spatiotemporal contributions to the spot size evolution. The spot size, therefore, evolves primarily through diffraction and self-focusing and can be approximated by $w = w_0[1 + (1 - \tilde{P})\tilde{L}^2]^{1/2}$, where $\tilde{L} = L/Z_R$ and $Z_R = \pi w_0^2/\lambda_L$ is the Rayleigh length, $\tilde{P} = P/P_{cr}$ is the ratio of the pulse power $P = \frac{1}{2}\pi w_0^2 I$ to the self-focusing critical power $P_{cr} = \lambda^2/2\pi n_{2,\text{eff}}$ and $n_{2,\text{eff}}$ is an effective nonlinear refractive index. The validity condition then becomes $|1 - \tilde{P}|\tilde{L}^2 \ll 1$. This condition is clearly satisfied when $\tilde{P} \simeq 1$, but this scenario requires equal power at every temporal slice in the pulse, for instance, a flat top temporal profile. Instead, we exploit the limit $\tilde{P} \gg 1$, providing the condition $n_{2,\text{eff}} I (L/w_0)^2 \ll 1$. Setting $n_{2,\text{eff}} = n_{2,\text{long}}$, the adiabatic value presented in Ref. [7], $I = 1 \times 10^{12}\text{W/cm}^2$, $\lambda_L = 8.4\mu\text{m}$, $L = 3\text{m}$, $w_0 = 1\text{cm}$, we have $\tilde{P} = 5.4$ and $n_{2,\text{eff}} I (L/w_0)^2 = 0.035$, satisfying the validity condition.

-
- [1] P. Sprangle, J. R. Penano, and B. Hafizi, Propagation of intense short laser pulses in the atmosphere, *Phys. Rev. E* **66**, 046418 (2002).
- [2] A. Couairon and A. Mysyrowicz, Femtosecond filamentation in transparent media, *Phys. Rep.* **441**, 47 (2007).
- [3] J. P. Palastro, Time-dependent polarization states of high-power ultrashort laser pulses during atmospheric propagation, *Phys. Rev. A* **89**, 013804 (2014).
- [4] C. H. Lin, J. P. Heritage, T. K. Gustafson, R. Y. Chiao, and J. P. McTague, Birefringence arising from the reorientation of the polarizability anisotropy of molecules in collisionless gases, *Phys. Rev. A* **13**, 813 (1976).
- [5] Y.-H. Chen, S. Varma, A. York, and H. M. Milchberg, Single-shot, space- and time-resolved measurement of rotational wavepacket revivals in H_2 , D_2 , N_2 , O_2 , and N_2O , *Opt. Express* **15**, 11341 (2007).
- [6] J. P. Palastro, T. M. Antonsen, Jr., and A. Pearson, Models of the delayed nonlinear Raman response in diatomic gases, *Phys. Rev. A* **84**, 013829 (2011).
- [7] J. K. Wahlstrand, Y.-H. Cheng, and H. M. Milchberg, Absolute measurement of the transient optical nonlinearity in N_2 , O_2 , N_2O , and Ar, *Phys. Rev. A* **85**, 043820 (2012).
- [8] R. A. Bartels, S. Backus, M. M. Murnane, and H. C. Kapteyn, Impulsive stimulated Raman scattering of molecular vibrations using nonlinear pulse shaping, *Chem. Phys. Lett.* **374**, 326 (2003).
- [9] J. H. Odnher, D. A. Romanov, and R. J. Levis, Self-Shortening Dynamics Measured Along a Femtosecond Laser Filament in Air, *Phys. Rev. Lett.* **105**, 125001 (2010).
- [10] A. M. Zheltikov, A. A. Voronin, R. Kienberger, F. Krausz, and G. Korn, Frequency-Tunable Multigigawatt Sub-Half-Cycle Light Pulses from Coupled-State Dynamics of Optical Solitons and Impulsively Driven Molecular Vibrations, *Phys. Rev. Lett.* **105**, 103901 (2010).
- [11] X. Chen, P. Polynkin, and M. Kolesik, Raman effect in self-focusing of few-cycle laser pulses in air, *Opt. Lett.* **38**, 2017 (2013).

- [12] J. K. Wahlstrand, S. Zahedpour, Y.-H. Cheng, J. P. Palastro, and H. M. Milchberg, Absolute measurement of the ultrafast nonlinear electronic and rovibrational response in H_2 and D_2 , *Phys. Rev. A* **92**, 063828 (2015).
- [13] W. Demtröder, *Molecular Physics* (Wiley-VCH, Weinheim, 2005).
- [14] B. Shim, S. E. Schrauth, and A. L. Gaeta, Filamentation in air with ultrashort mid-infrared pulses, *Opt. Express* **19**, 9118 (2011).
- [15] D. Kartashov, S. Alisauskas, A. Pugzlys, A. Voronin, A. Zheltikov, M. Petrarca, P. Bejot, J. Kasparian, J.-P. Wolf, and A. Baltuska, Mid-infrared filamentation in molecular gases, *Opt. Lett.* **38**, 3194 (2013).
- [16] A. V. Mitrofanov, A. A. Voronin, D. A. Sidorov-Biryukov, A. Pugžlys, E. A. Stepanov, G. Andriukaitis, T. Flöry, S. Ališauskas, A. B. Fedotov, A. Baltuška, and A. M. Zheltikov, Mid-infrared laser filaments in the atmosphere, *Sci Rep.* **5**, 8368 (2015).
- [17] S. Zahedpour, J. K. Wahlstrand, and H. M. Milchberg, Measurement of the nonlinear refractive index of air constituents at mid-infrared wavelengths, *Opt. Lett.* **40**, 5794 (2015).
- [18] P. Panagiotopoulos, P. Whalen, M. Kolesik, and J. V. Moloney, Super high power mid-infrared femtosecond light bullet, *Nat. Photonics* **9**, 543 (2015).
- [19] R. W. Boyd, *Nonlinear Optics*, 3rd ed. (Academic, Burlington, MA, 2008).
- [20] W. F. Murphy, W. Holzer, and H. J. Bernstein, Gas phase raman intensities: A review of “pre-laser” data, *Appl. Spectroscopy* **23**, 211 (1969).
- [21] J. K. Wahlstrand, J. H. Odnher, E. T. McCole, Y.-H. Cheng, J. P. Palastro, R. J. Levis, and H. M. Milchberg, Effect of two-beam coupling in strong-field optical pump-probe experiments, *Phys. Rev. A* **87**, 053801 (2013).
- [22] J. P. Palastro, T. M. Antonsen, Jr., and H. M. Milchberg, Compression, spectral broadening, and collimation in multiple, femtosecond pulse filamentation in atmosphere, *Phys. Rev. A* **86**, 033834 (2012).
- [23] M. Kolesik and J. V. Moloney, Nonlinear optical pulse propagation simulation: From Maxwell’s to unidirectional equations, *Phys. Rev. E* **70**, 036604 (2004).
- [24] A. Couairon, E. Brambilla, T. Corti, D. Majus, O. de J. Ramirez-Gongora, and M. Kolesik, Practitioner’s guide to laser pulse propagation models and simulation, *Eur. Phys. J.: Spec. Top.* **199**, 5 (2011).
- [25] R. J. Mathar, Refractive index of humid air in the infrared: model fits, *J. Opt. A: Pure Appl. Opt.* **9**, 470 (2007).
- [26] S. V. Popruzhenko, V. D. Mur, V. S. Popov, and D. Bauer, Strong Field Ionization Rate for Arbitrary Laser Frequencies, *Phys. Rev. Lett.* **101**, 193003 (2008).
- [27] A. Talebpour, J. Yang, and S. L. Chin, Semi-empirical model for the rate of tunnel ionization of N_2 and O_2 , molecule in an intense Ti:sapphire laser pulse, *Opt. Commun.* **163**, 29 (1999).